

Northumbria Research Link

Citation: Yu, Xin, Wu, Zijian, Weng, Ling, Jiang, Dawei, Algadi, Hassan, Qin, Zhuofan, Guo, Zhanhu and Xu, Bin (2023) Flexible strain sensor enabled by carbon nanotubes-decorated electrospun TPU membrane for human motion monitoring. *Advanced Materials Interfaces*, 10 (11). p. 2202292. ISSN 2196-7350

Published by: Wiley-Blackwell

URL: <https://doi.org/10.1002/admi.202202292>
<<https://doi.org/10.1002/admi.202202292>>

This version was downloaded from Northumbria Research Link:
<https://nrl.northumbria.ac.uk/id/eprint/51265/>

Northumbria University has developed Northumbria Research Link (NRL) to enable users to access the University's research output. Copyright © and moral rights for items on NRL are retained by the individual author(s) and/or other copyright owners. Single copies of full items can be reproduced, displayed or performed, and given to third parties in any format or medium for personal research or study, educational, or not-for-profit purposes without prior permission or charge, provided the authors, title and full bibliographic details are given, as well as a hyperlink and/or URL to the original metadata page. The content must not be changed in any way. Full items must not be sold commercially in any format or medium without formal permission of the copyright holder. The full policy is available online: <http://nrl.northumbria.ac.uk/policies.html>

This document may differ from the final, published version of the research and has been made available online in accordance with publisher policies. To read and/or cite from the published version of the research, please visit the publisher's website (a subscription may be required.)

Flexible Strain Sensor Enabled by Carbon Nanotubes-Decorated Electrospun TPU Membrane for Human Motion Monitoring

Xin Yu, Zijian Wu,* Ling Weng,* Dawei Jiang, Hassan Algadi, Zhuofan Qin, Zhanhu Guo,* and Ben Bin Xu*

High-performance flexible strain sensors are gaining more and more attention with their bespoke detection range, excellent sensing performance, and good stability, which are highly desired in wearable electronics. Herein, a thermoplastic polyurethane elastomer (TPU) fibrous membrane is prepared as a flexible substrate by electrostatic spinning technology, then a coating of polydopamine is formed through fast synthesizing the dopamine on TPU fibrous membrane surface and loaded with carbon nanotubes (CNTs) to develop an extremely sensitive flexible strain sensor. The flexible sensor prepared by TPU fibrous membrane coated with polydopamine layer has an outstanding sensitivity under the pulling force (Gauge Factor of 10 528.53 with 200% strain), rapid reaction time (188–221 ms), wide sensing range (up to 200%), good stability, and durability. The theoretical studies reveal the underlying cause for the high sensitivity and the inherent relationship between the amount of conducting routes and the length between adjacent conducting fillers in the sensor. The demonstration of the device shows a promising application to sense human motion at various locations of the body, with the accurate and stable electrical signal output generated at corresponding motion.

of encouraging utilization in the areas of human motion monitoring, flexible electronic skin, medical diagnosis, and human-machine interface.^[7–19] Conventional sensors are composed of rigid materials, which are hard and brittle in texture and difficult to curl, and cannot meet the applications in some specific fields, which require stretchable conductors that can maintain stable electrical conductivity even when undergoing large deformations. Conductive polymer composites (CPCs) have good flexibility and good tensile properties to meet the environment of sensors under large tensile (strain \geq 50%) and bending conditions.

Common flexible strain sensors choose flexible polymer materials with good stretchability as substrate layer, including polydimethylsiloxane (PDMS),^[20–24] thermoplastic polyurethane elastomer (TPU),^[25–27] and Ecoflex.^[28,29] Commonly, flexible strain sensors usually incorporate


nanometals (such as metal nanoparticles, silver nanowires),^[30–32] nanocarbon materials (including carbon black, CNTs, graphene, etc.),^[33–45] conductive polymers (including PANI, PPy, and PEDOT:PSS),^[46–49] and other conducting materials like Mxene^[50–52] as conductive fillers with polymeric

1. Introduction

With the advent of a new era of flexible wearable devices, strain sensors have gradually become a hot spot of attention in academia and industry.^[1–6] Strain sensors have a broad range

X. Yu, Z. Wu, L. Weng
 Department of Material Science and Technology
 Harbin University of Science and Technology
 Harbin 150040, China
 E-mail: zijian.wu@hrbust.edu.cn; l.weng@hrbust.edu.cn

Z. Wu, L. Weng
 Key Laboratory of Engineering Dielectric and Its Application
 Technology of Ministry of Education
 Harbin University of Science and Technology
 Harbin 150040, China

 The ORCID identification number(s) for the author(s) of this article can be found under <https://doi.org/10.1002/admi.202202292>.

© 2023 The Authors. Advanced Materials Interfaces published by Wiley-VCH GmbH. This is an open access article under the terms of the Creative Commons Attribution License, which permits use, distribution and reproduction in any medium, provided the original work is properly cited.

DOI: 10.1002/admi.202202292

D. Jiang
 Heilongjiang Key Laboratory of Molecular Design
 and Preparation of Flame Retarded Materials
 Northeast Forestry University
 Harbin 150040, China

H. Algadi
 Department of Electrical Engineering
 Faculty of Engineering
 Najran University
 Najran 11001, Saudi Arabia

H. Algadi
 College of Materials Science and Engineering
 Taiyuan University of Science and Technology
 Taiyuan 030024, China

Z. Qin, Z. Guo, B. B. Xu
 Mechanical and Construction Engineering
 Faculty of Engineering and Environment
 Northumbria University
 Newcastle Upon Tyne NE1 8ST, UK
 E-mail: zhanhu.guo@northumbria.ac.uk; ben.xu@northumbria.ac.uk

substrates to impart excellent electrical conductivity to the composites.

A broad detection range and a lower monitoring limit are key criteria for a stretchable and flexible strain sensor. A low monitoring limit of the sensor allows a fast and accurate response to a small strain stimulus, which is crucial for real-time monitoring of human motions and human health. The wider detection range can satisfy the use of a sensor at a larger strain. In recent years, electrostatic spinning has been widely used as a micro/nanofiber preparation technology due to its preparation of electrospinning membranes with a big specific surface area, large porosity, good mechanical flexibility, and its simple and efficient preparation method.^[53–57] Among them, TPU is simply electrostatically spun into fibrous membranes, that exhibit excellent tensile properties, flexibility, and mechanical strength.^[58,59] As a kind of emerging nanomaterials, CNTs are also widely used in many fields.^[60–64] Selecting suitable materials to prepare various sensors has become the research focus of scholars at home and abroad.^[65–71] Li et al.^[72] prepared a flexible sensor with a wide monitoring range and ultralow detection limit by ultrasonically anchoring CNTs to TPU electrospun membrane. However, it also shows the disadvantage of a low sensitivity limit, which is less desirable in a condition requiring high sensitivity. The flexible sensors with high sensitivity, good responsiveness, and a wide detection range remain yet to be developed.

In this work, TPU fibrous membrane was prepared as a flexible substrate by electrostatic spinning, and the TPU fibrous membrane was coated with dopamine (DA) self-polymerization (named DT), and CNTs particles were introduced on the substrate by filtration to build the conductive layer (coded as CT and CDT). We systematically studied the impact of introducing a polydopamine layer on the conductive layer, the surface morphologies of the CT sensor as well as the CDT sensor, the mechanical properties of the CT and CDT samples, and the differences in sensing properties during stretching, and the mechanical hysteresis of this samples with the dependencies on different substrate structures.^[73–75] A mathematical model leads the understanding of the variation of resistance with strain ($\Delta R/R_0$) by using tunneling theory, and is used to analyze the sensitivity between CT and CDT samples caused by the length of neighboring conductive fillers and the amount of conducting routes was analyzed to provide an expla-

nation by calculating the parameters of this mathematical model. The final prepared CDT sensor has a low detection limit (<1%), a broad detecting range (up to 200%), an extremely high sensitivity (Gauge Factor of 10 528.53 at 200% strain), and great cycle stability due to the presence of the polydopamine layer, which can respond accurately to various human movements and even vocalizations.

2. Result and Discussion

2.1. Preparation of High Sensitivity Sensor

The preparation of stretchable CNTs/DA/TPU flexible strain sensor is illustrated in **Figure 1**, the experimental details are described in Section 4. We assign a code name of CT for the CNT-coated TPU flexible strain sensor, and CDT for CNTs/DA/TPU flexible strain sensor.

The morphology of the prepared conductive fibrous membranes is revealed in **Figure 2**. The surface of pure TPU fibers appears to be relatively even (Figure 2a,b), a small amount of CNTs was loaded on the surface of TPU fibers after binding with CNTs (Figure 2e,f). The surface of DATPU prepared after dopamine coating was rougher (Figure 2c,d), and was completely coated by CNTs after binding with CNTs (Figure 2g,h). This may be caused by that DA underwent self-polymerization on the TPU surface to form a polydopamine layer and uniformly coated the TPU fibers, which increased the roughness of the fiber surface and was able to bind more CNTs to the surface of the fiber when pumping the same content of CNTs suspension.

The loading of carbon nanotubes plays a critical role in determining the conductivity of the fibrous membrane. CNTs suspensions of (2.5 mL/5 mL/7.5 mL/10 mL/15 mL) with a concentration of 2 g L⁻¹ were pumped onto TPU electrospun membranes to control the loading of CNTs. The relative resistance of CNTs/TPU flexible strain sensors with different CNTs loadings at 10–50% strain is shown in **Figure 3a**. The relative resistance of CNTs/TPU flexible sensors showed an increasing trend at 10% and 30% strain with increasing CNT loadings, but the maximum relative resistance of flexible strain sensors with 15 mL of CNTs suspension pumped at 50% strain was about

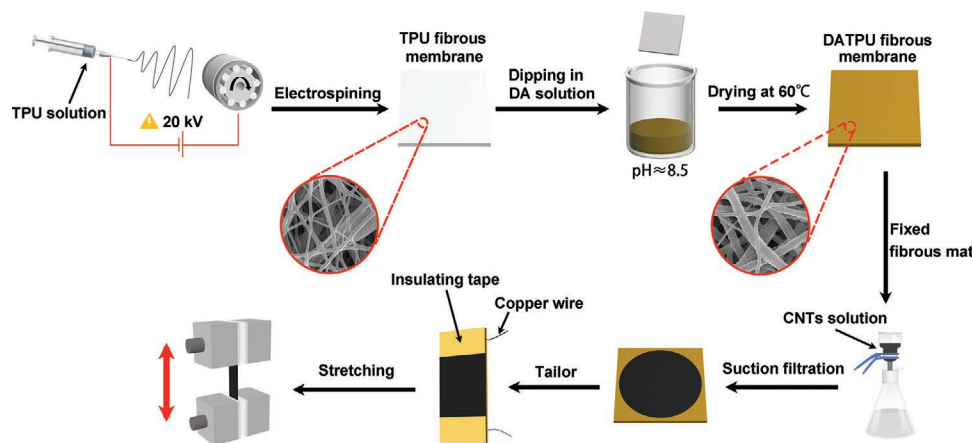


Figure 1. Schematic diagram of the preparation of CNTs/DA/TPU flexible strain sensor.

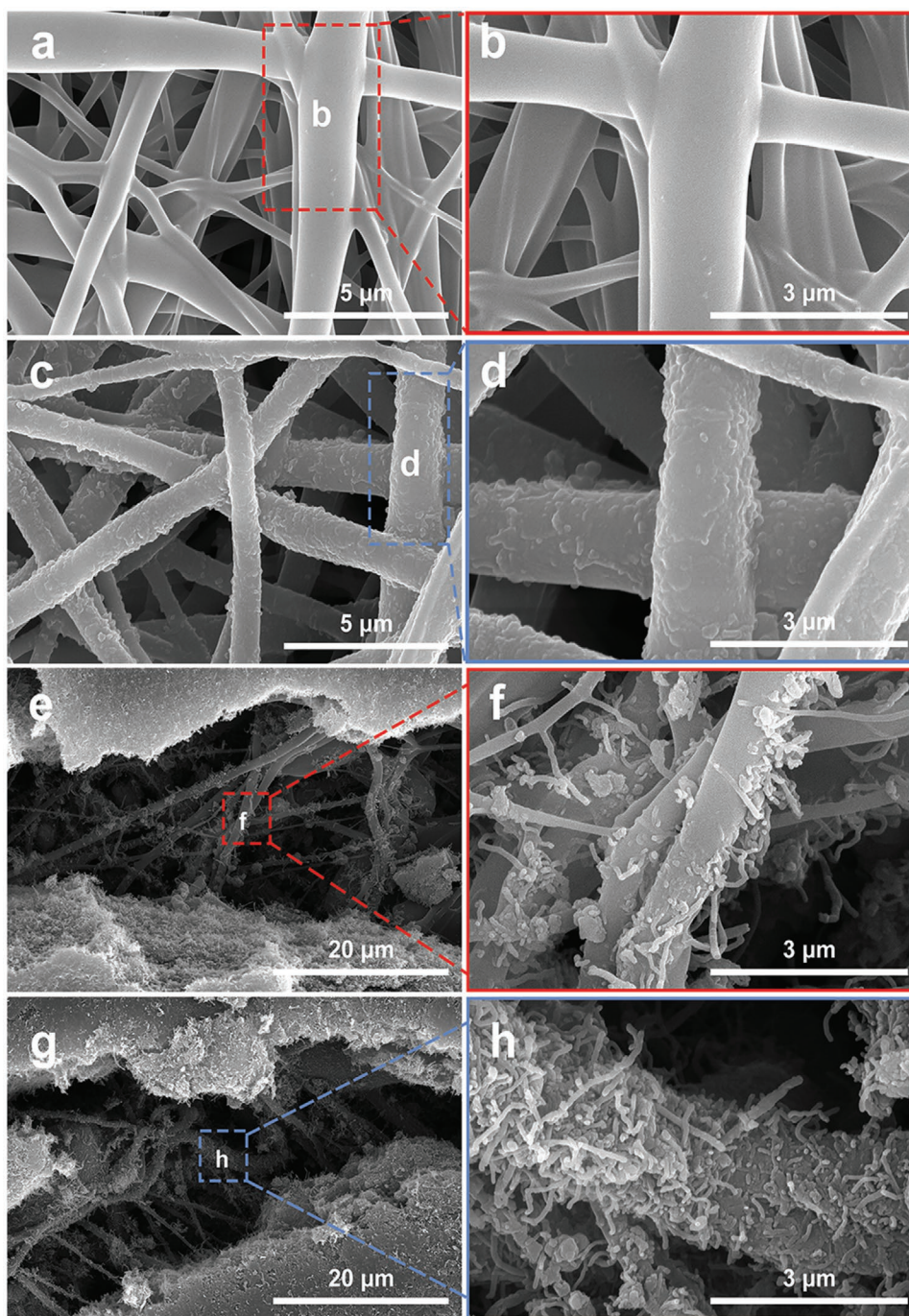


Figure 2. a,b) TPU electrospun membrane, c,d) DA/TPU fibrous membrane, e,f) CNTs/TPU flexible strain sensor, g,h) scanning electron microscope images of CNTs/DA/TPU flexible strain sensor.

38.39. However, the maximum relative resistance of a flexible sensor with 15 mL of CNTs suspension at 50% strain was about 38.39, while the maximum relative resistance of a flexible sensor with 10 mL of CNTs suspension is about 59.62, indicating a significant decrease in the relative resistance.

The hypothetical reason is that the specimen underwent the process of destruction and reconstruction of conducting network with cyclic stretching, the conductive pathway constructed on the TPU

substrate gradually increased as the load of CNTs increased, and the destruction of the conductive pathway increased at the same strain. However, when the loading of CNTs continues to increase to a certain amount, most conductive pathways are still not completely destroyed under larger strains, and the conductive networks of conductive fillers are still lapped, causing a significant decrease in relative resistance. A flexible strain sensor with a 10 mL suspension of CNTs was considered to be an optimal set for the application.

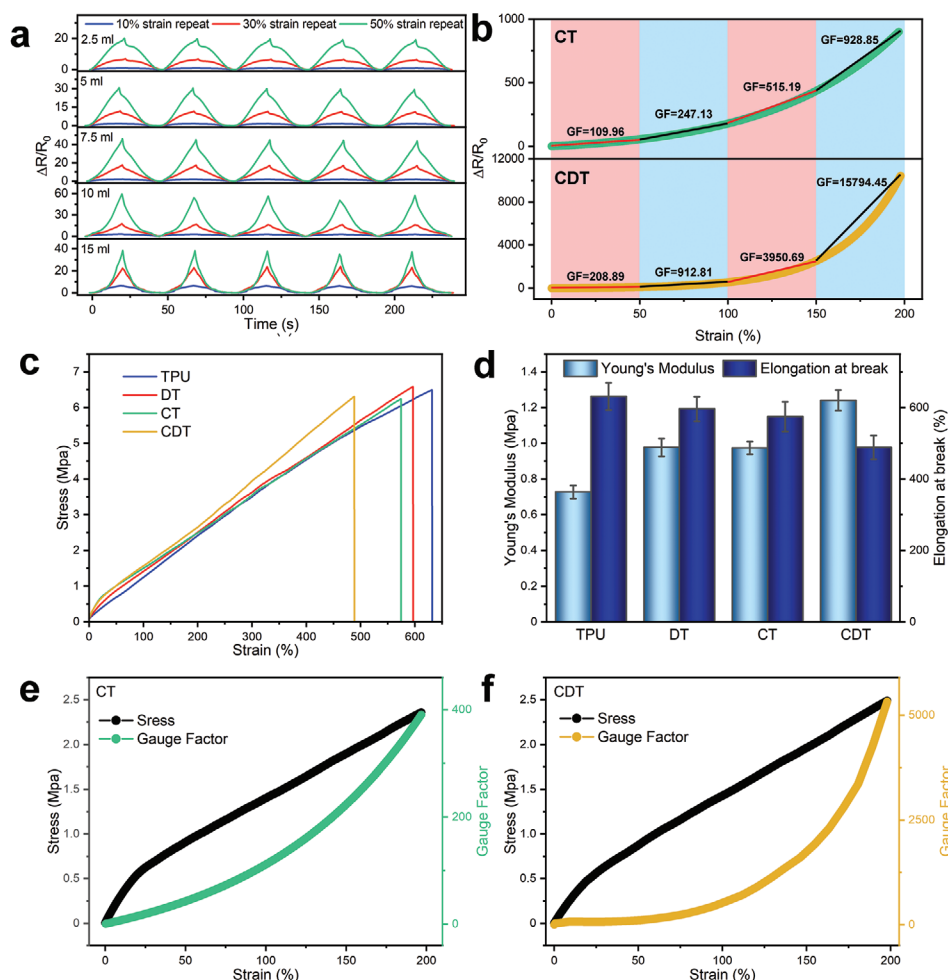


Figure 3. a) The relative resistance of CNTs/TPU flexible strain sensors at 10%, 30%, and 50% strain at CNTs draws from 2.5 to 15 mL, b) sensitivity of CT sensors and CDT sensors in four regions from 0–200% strain, c) typical stress-strain curves, d) Young's modulus of TPU, DT, CT, and CDT samples and fracture Elongation, e,f) Sensitivity of CT and CDT sensors at 0–200% tensile range per unit strain (GF).

2.2. Mechanical Properties and Sensing Performance of CT and CDT Flexible Strain Sensors

We further studied the strain sensing performance and mechanism of high gauge factor in the CT and CDT sensors. In general, the GF (Gauge Factor) is a crucial parameter to assess the sensing performance, identified as the ratio of relative resistance change to strain, and can be calculated by Equation (1)

$$GF = (\Delta R/R_0)/\varepsilon, \varepsilon = \Delta L/L_0 \quad (1)$$

where the R_0 and ε are the initial resistance and applied strain, respectively. ΔR is the difference between the real-time resistance and the initial resistance.

Figure 3b compares the sensitivity of CT and CDT flexible strain sensors in four regions from 0–200% strain, where the GF values of CT flexible strain sensor are 109.96 (0–50% strain), 247.13 (50–100% strain), 515.19 (100–150% strain), and 928.85 (150–200% strain), respectively. The GF values of CDT

flexible strain sensors were 208.89 (0–50% strain), 912.81 (50–100% strain), 3950.69 (100–150% strain), and 15 794.45 (150–200% strain). It can be observed that the gauge factors of the CDT sensor are higher than those of the CT sensor in all strain regions, empowered by the polydopamine layer-wrapped fiber surface. Figure 3c shows the typical stress-strain curves of the conductive composite fibrous membrane, the tensile strength of the prepared pure TPU fibrous membrane is 6.49 ± 0.12 MPa, and the tensile strength of the DATPU fibrous membrane is 6.58 ± 0.11 MPa, the tensile strength of the dopamine-coated TPU fibrous membrane is increased by about 0.1 MPa. In addition, the tensile strength of the prepared CT sensor is 6.24 ± 0.21 MPa for the CT sensor and 6.31 ± 0.15 MPa for the CDT sensor, it can be observed that the tensile strength of the TPU fibrous membrane increased after being coated with dopamine, which interacts more strongly with it.

In addition, Young's modulus of pure TPU fibrous membrane in Figure 3d reached 0.73 MPa and the elongation at break was $631\% \pm 37\%$. Young's modulus of the DATPU fiber

membrane reached 0.98 MPa and the elongation at break was $596\% \pm 34\%$. With the introduction of dopamine, Young's modulus of fibrous membranes increased significantly, however, the elongation at break decreased, probably due to the strong bonding ability between the PDA coating and TPU fibers and the strong inter- and intramolecular hydrogen bonding exhibited by both the PDA coating and the PDA and TPU matrix.^[76] Also compared to CT (Young's modulus 0.97 MPa, elongation at break $574\% \pm 33\%$), Young's modulus of CDT was more significantly improved by 0.27 MPa with a Yang's modulus of 1.24 MPa, nevertheless, its elongation also decreased significantly with a CDT elongation at break of $488\% \pm 30\%$, which could be attributed to the polydopamine layer and more CNTs attached between the fibers, which helps to reduce the slip between fibers.^[77] To further compare the sensitivity of CT sensor with that of the CDT sensor, the GFs of both sensors were compared at 0–200% strain, corresponding to 399.66 and 5322.82 for CT and CDT, respectively, further illustrating the better responsiveness of CDT (Figure 3e,f).

2.3. Mechanical Hysteresis of Strain Sensor

The long-term stability, as well as the durability of sensors, are important for applications in detecting real-time motion. Figure 4a,b shows the cyclic loading and unloading curves for 20 cycles at 10% strain for the CT and CDT sensors, respectively, with the red line showing the first cycle and the blue line showing cycles 2–20. Mechanical hysteresis (H_M) is an effective indicator to guide the construction of an internal conductive network of CT and CDT sensors, as we need to minimize H_M when the sensors undergo multiple loading and unloading cycles.^[73,74] From Figure 4c, the ($A_L - A_U$) area and the A_U area are represented in orange and green, respectively. The H_M value could be measured from Equation (2) as follows:

$$H_M = \frac{|A_L - A_U|}{A_L} \quad (2)$$

where A_L is the integral area of the loading curve to the x -axis and A_U is the integral area of the unloading curve to the x -axis.

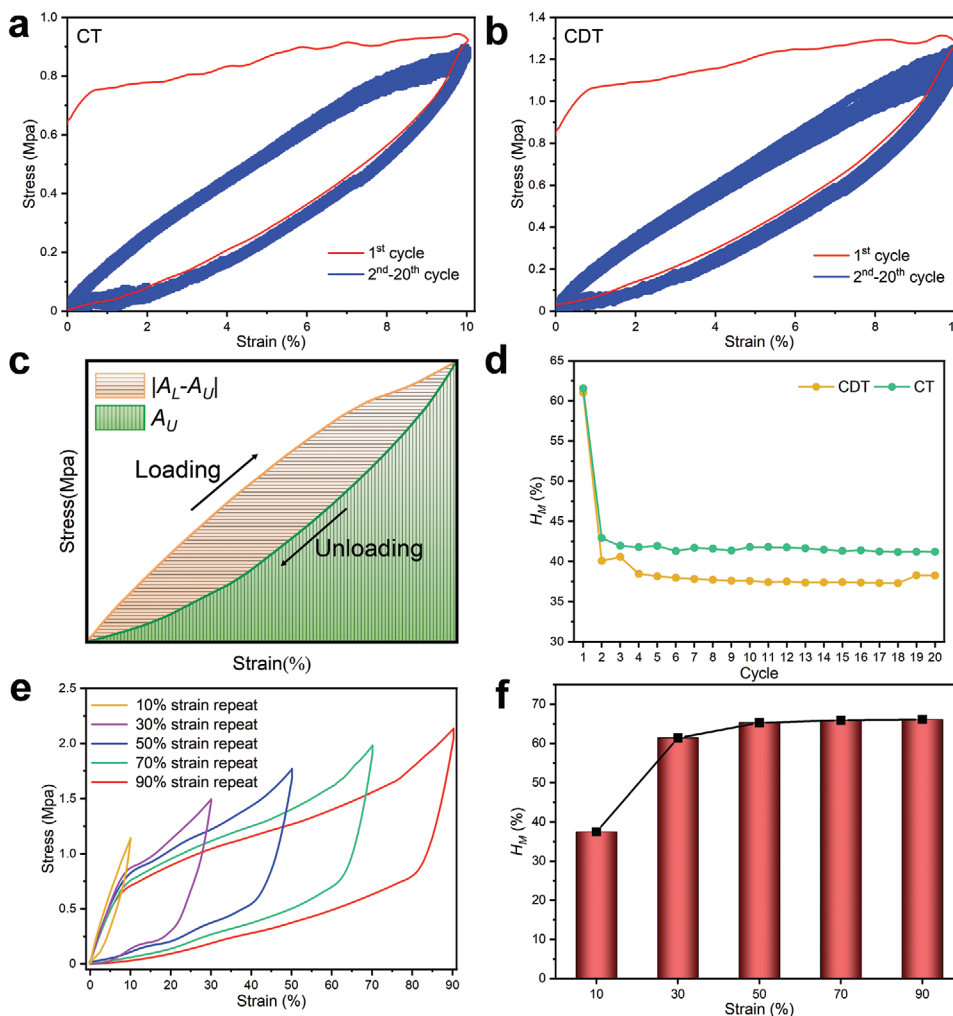


Figure 4. a,b) Cyclic stress-strain curves of CT and CDT sensors at 10% strain, c) mechanical hysteresis (H_M) quantification schematic, d) H_M of CT and CDT sensors at 10% strain for 20 cycles of stretching, e) cycling stress-strain curves of CDT sensors at the strain range of 10–90%, f) H_M of CDT sensors at 10–90% strain for cyclic stretching.

The H_M of the CT and CDT sensors were calculated separately for 20 cycles at 10% strain in Figure 4d. The results showed that the polydopamine-coated fibrous membrane exhibited a lower H_M . During the first cycle, the H_M was 61.53% and 60.99% for the CT and CDT, respectively, with little difference. However, during the 2–20 cycles, the average H_M of CT and CDT decreased to 41.60% and 37.97%, respectively. This is due to the plastic deformation as well as the elastic deformation of TPU during the stretching–recovery process. In the first loading and unloading process, the conductive pathways of CNTs fractured for the first time, resulting in higher tensile stress in the first loading curve. In the process of unloading, TPU fibrous membrane returned to its initial state and without any distortion, thus exhibiting a relatively high H_M .^[68] The sensors underwent the same process during subsequent stretching as well as recovery, but the plastic deformation of the TPU under external forces during unloading was permanent owing to the hysteresis effect of the composite and stabilized the H_M of the samples after several stretching cycles.^[73,74]

The CDT sensor exhibited a lower H_M during subsequent cycles, indicating that the CDT sample exhibited lower energy consumption as well as more excellent long-term durability than the CT sample during multiple cycles of stretching. Figure 4e,f shows the twentieth cyclic stress–strain curves of the CDT sensor at five strains from 10% to 90% and their corresponding H_M , respectively. The data demonstrate that the H_M of the sensor at 30%, 50%, 70%, and 90% strains do not differ significantly, further demonstrating the good cyclic stability of the CDT sensor.

2.4. Theoretical Understanding of Conductive Fillers Enabled Strain Sensing

Figure 5a exhibits the CNTs content as well as the polydopamine layer coated on TPU in CT as well as CDT sensors determined by thermogravimetric analysis (TGA), which can be calculated by the following equation

$$m_{CT} = m_{CNTs1} + m_{TPU} \quad (3)$$

$$b \cdot m_{CT} = m_{CNTs1} + a \cdot m_{TPU} \quad (4)$$

$$W_{CNTs1} = \frac{m_{CNTs1}}{m_{CT}} = \frac{b-a}{1-a} \quad (5)$$

$$m_{DT} = m_{DA} + m_{TPU} \quad (6)$$

$$c \cdot m_{DT} = m_{DA} + a \cdot m_{TPU} \quad (7)$$

$$W_{DA} = \frac{m_{DA}}{m_{DT}} = \frac{c-a}{1-a} \quad (8)$$

$$m_{CDT} = m_{CNTs2} + m_{DT} \quad (9)$$

$$d \cdot m_{CDT} = m_{CNTs2} + c \cdot m_{DT} \quad (10)$$

$$W_{CNTs2} = \frac{m_{CNTs2}}{m_{CDT}} = \frac{d-c}{1-c} \quad (11)$$

where m_{TPU} , m_{CNTs} , m_{DA} , and m_{DT} are the weights of pure TPU fibrous membrane, carbon nanotubes, dopamine layer, and DATPU fibrous membrane in the sensor, respectively. m_{CT} and m_{CDT} are the total weights of the CT sensor and CDT sensor, respectively. For the CT sensor, the residual weight ratio of the pure TPU fibrous membrane measured after thermal degradation of the sample is a and the residual weight ratio of the CT sensor is b . Therefore, the content of CNTs in the CT sensor (W_{CNTs1}) is calculated as 15.55% according to Equation (5). For the CDT sensor, the residual thermogravimetric ratio of DATPU after thermal degradation of the sample is c , and the residual weight ratio of the CDT sensor is d . First, the content of dopamine (W_{DA}) coated on TPU fiber can be calculated as 0.9% according to Equation (8), and then the content of CNTs in the CDT sensor (W_{CNTs2}) can be calculated by Equation (11) as 17.73%. The results show that the loading of CNTs in the CDT sensor is higher than that in the CT sensor, which can further indicate that the roughness of the fiber surface can be increased due to the coating of the polydopamine layer on the TPU fibers, and more CNTs can be anchored on the fiber surface. Due to the strong interaction between the –OH in the polydopamine layer and the –COOH in the CNTs, more CNTs are anchored on the fiber surface.^[78–80]

2.5. Resistance Fitting Model for Sensors

The attachment of polydopamine onto the TPU fiber surface has a significant effect on the formation of the conductive network. At the microstructural level, the total resistance of CT as well as CDT sensors can be seen as a function of the R of every conducting filler and the resin matrix.^[12,81] The conductive fillers and conductive paths in the conductive network can be visualized as a function of the total resistance by means of a relationship curve between relative resistance and strain. The following equation is used to express the total resistance Equation (12).^[75]

$$R = \frac{M(R_m + R_c)}{N} \quad (12)$$

where R , R_m , and R_c are the total resistance of the final composite, the resistance between two neighboring conductive fillers, and the resistance of a single conductive filler, respectively. For electrically conductive composites, R_m is far greater than R_c , so $R_m + R_c \approx R_m$. M is the amount of fillers building a conductive path and N is the amount of conductive paths formed. On the basis of the tunneling effect theory, the resistance relationship can be expressed by the following equation.^[12,82]

$$R_m = \frac{8\pi h s}{3c^2 r e^2} \exp(rs), r = \frac{4\pi}{h} \sqrt{2m_e \phi} \quad (13)$$

Substituting Equations (3–13) into (3–12) gives

$$R = \frac{M}{N} \left[\frac{8\pi h s}{3c^2 r e^2} \exp(rs) \right] \quad (14)$$

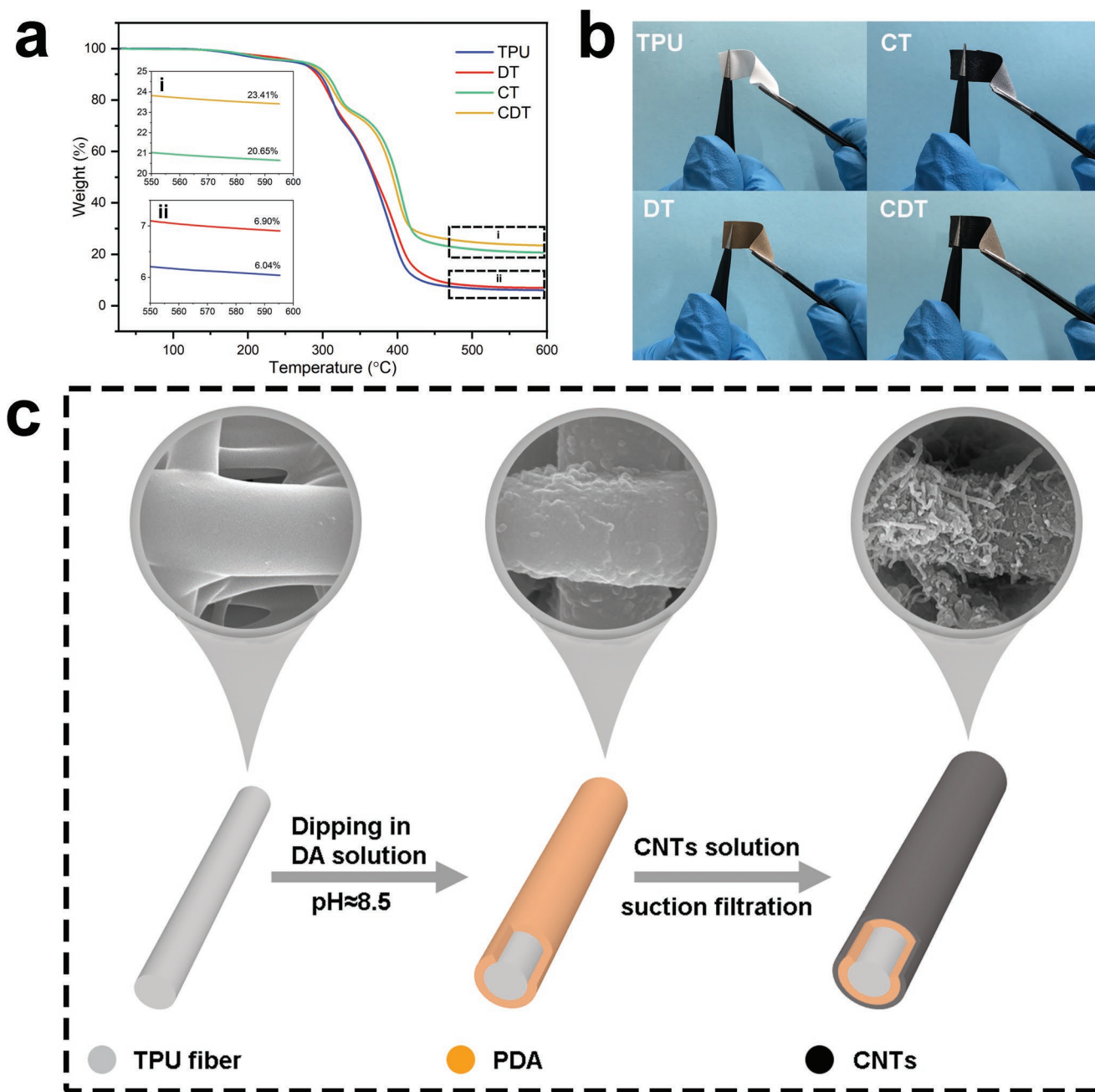


Figure 5. a) Thermogravimetric analysis of pure TPU fibrous membrane, DT fibrous membrane, CT, and CDT sensor, b) optical photos of four samples, c) demonstration of a single fiber during CDT sensor preparation.

where h is Planck's constant, c^2 is the effective cross-section, e is the electron charge, s is the average distance between neighboring conducting fillers, m_e is the electron mass, and φ is the height of tunneling potential barrier.

As stress is applied to the sensor, the tunneling distance between CNTs particles increases, and there is a process of destruction and reconstruction of the conducting path within the conducting network. Assuming that the tunneling distance between neighboring conducting particles satisfies a linear function from s_0 to s and the number of conducting paths

satisfies an exponential function from N_0 to N , they can be calculated as follows:

$$s = s_0 (1 + Ax) \quad (15)$$

$$N = N_0 \exp[f(x)] \quad (16)$$

where s_0 and N_0 are the initial conductive particle distance and the initial conductive path number, respectively. x is the applied strain and $f(x)$ is a function of the strain x . A is a constant that

relies on the type of conductive filler and the measurement conditions. $\Delta R/R_0$ can be obtained by substituting Equation (17).

$$\frac{\Delta R}{R_0} = \frac{R - R_0}{R_0} = \frac{R}{R_0} - 1 = \left(\frac{s}{s_0} \times \frac{N_0}{N} \right) \exp[r(s - s_0)] - 1 \quad (17)$$

$$= (1 + Ax) \exp[r(s - s_0) - f(x)] - 1$$

where $[r(s - s_0) - f(x)]$ can be used to express the relationship between the tunneling potential height (φ) and the number of varying conducting paths (N), as Equation (18):

$$bx^c = [r(s - s_0) - f(x)] \quad (18)$$

Substituting Equation (18) into Equation (17), $\Delta R/R_0$ can then be expressed as a function of strain x , as shown in Equation (19).

$$\frac{\Delta R}{R_0} = (1 + Ax) \exp(bx^c) - 1 \quad (19)$$

where A , b , and c are constants.

For Equation (16), in the actual stretching case, the conductive path of the sensor will be gradually broken upon stretching, the number of conductive paths will gradually decrease with rising strain until all conductive paths break ($N \rightarrow 0$) and the sensor conductive failure, the calculation limit of which is shown below

$$f(x) = \ln \frac{N}{N_0} \quad (20a)$$

$$\lim_{N \rightarrow 0} f(x) = \lim_{N \rightarrow 0} \ln \frac{N}{N_0} = -\infty \quad (20b)$$

Then substituting $[f(x) \rightarrow -\infty]$ into Equation (16), we get

$$bx^c = [r(s - s_0) - f(x)] \approx -f(x) \quad (21)$$

$$\frac{N}{N_0} = \exp(-bx^c) \quad (22)$$

Figure 6a shows the experimental curve of $\Delta R/R_0$ depending on the strain fitted based on the model of Equation (19). These parameters (A , b , c) calculated from the experimental test results and R^2 are shown in Table 1. The calculated data indicate that the model Equation (19) can well verify and describe the relative resistance versus strain of CT as well as CDT sensors, and matches well with the actual test results. Figure 6b,c shows the simulated conductive path variation ratio N/N_0 and conductive interparticle distance variation ratio s/s_0 versus strain based on the parameters in Table 1 and Equations (22) and (15). In Figure. 6b, according to the fitting results, it can be seen that when the strain reaches 200%, the N/N_0 of the CT sample is 0.14 and the N/N_0 of the CDT sample is 0.02. It could be observed that the number of conducting paths of the CDT sample is closer to 0 at 200% strain, and the conductive paths

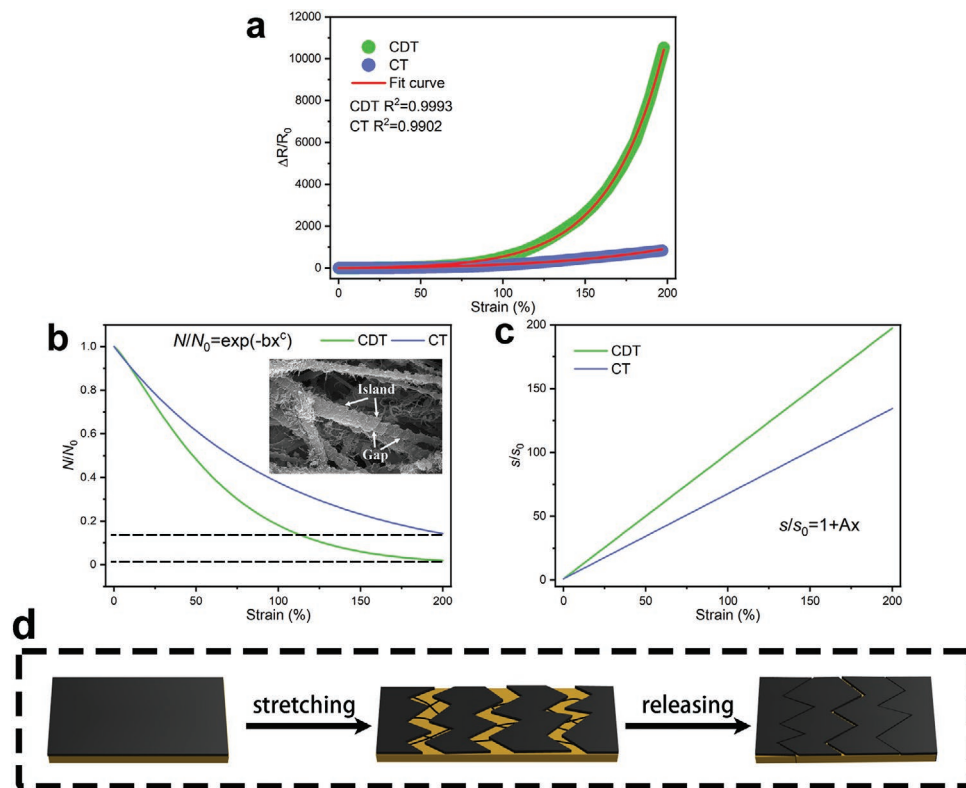


Figure 6. a) Fit function of $\Delta R/R_0$ versus strain for CT and CDT sensors and theoretical data, b) Fit function of conductive path number for CT and CDT sensors, c) Fit function of distance between conductive particles for CT and CDT sensors, d) Schematic diagram of CDT sensor operating principle.

Table 1. Model calculation parameters of Equation (19).

	<i>A</i>	<i>b</i>	<i>c</i>	<i>R</i> ²
CT	0.667 ± 0.20	0.010 ± 0.011	1.000 ± 0.184	0.9902
CDT	0.982 ± 0.25	0.062 ± 0.003	1.222 ± 0.065	0.9993

in the conductive network decrease faster, which may be due to the fact that the polydopamine layer is wrapped on the TPU fiber. During the stretching, the polydopamine layer cracked and formed a special lamellar structure on the surface of TPU nanofiber, which accelerated the migration of more CNTs loaded on the polydopamine layer, leading to a faster reduction in the number of conductive paths. In Figure 6c, the slope (s/s_0) for the CDT sample is greater, and the distance between the conducting particles changes faster, which well verifies the previous conjecture that the CDT sensor works as shown in Figure 6d.

Based on the numerical model constructed by Equation (19), the parameters (*A, b, c*) can visualize the level of change in the number of conductive paths and the level of change in the distance between conductive particles during the stretching process. For CT samples and CDT samples, the presence of polydopamine layers can affect the values of three parameters (Table 1). The parameter *A* represents the changing rate of the distance between the conducting fillers of adjacent CNTs, and the larger value of *A* for CDT samples compared to CT samples indicates that the distance between the conductive particles of CDT samples increases faster during stretching. Parameters *b* and *c* represent the change in conductive paths and are of great importance when analyzing the conductivity and sensitivity of the sensor. The larger values of *b* and *c* for the CDT samples compared to the CT samples indicate that the CDT samples have higher sensitivity. Normally, the interval between neighboring conducting fillers and conducting paths is difficult to measure. Equations (15) and (22) can accurately predict the change in distance between conductive fillers and the change in the number of conductive paths during the stretching. These mathematical models have been effective in predicting the change in conductive paths and neighboring conducting fillers.

2.6. Sensing Performance of CDT Sensors

Figure 7a,b shows the repetitive electrical signal response of the CDT sensor for ten cycles at 10%, 20%, and 30% strain and 50%, 70%, and 100% strain, respectively, and it can be seen that the prepared CDT sample has good responsiveness. Figure 7c,d shows the *I*–*V* curves of the CDT sensor at micro-strain (0–10%) and large strain (30–200%). The *I*–*V* curves of the CDT sample for a gradual increase of voltage from –6 to 6 V are in strict accordance with Ohm's law, which indicates good reliability.

Figure 7e shows the response time measured by rapidly stretching the CDT sensor at 1% strain with a stretching rate of 200 mm min^{–1}. At the loading stage, the resistance of the CDT sensor rises quickly after the strain is applied, and the response time is 188 ms. At the unloading stage, the resistance of the

CDT sensor declines quickly after the strain is withdrawn, and the response time is 221 ms, with a difference of 33 ms. The response time increases slightly in the unloading, which may be due to the fact that the recovery of the polydopamine layer wrapped on TPU fibers at a very fast stretching speed requires more time, leading to the delayed re-lap of the conductive network. Figure 7f shows three cycles of testing of the CDT sample from 10% to 190% strain at each strain increase of 20%. It could be observed that the CDT sensor responds accurately to each stage of strain, further verifying that the CDT sensor has good reliability. In Figure 7g, the CDT sensor was tested for 300 cycles at 10% strain at a stretching speed of 100 mm min^{–1}, and the results showed that the CDT sensor has good stability in long-term usage.

2.7. Application of CDT Sensors in Human Motion Monitoring

Based on the good stability and flexibility, high sensitivity, and fast response capability of the CDT sensor fabricated in this work, it can be employed to monitor the movement of the human body in real-time (Figure 8a–f). As illustrated in Figure 8a,b, the resistance of the CDT sensor gradually increases with the bending of the finger at different bending angles (30°, 60°, and 90°) and returns to the initial position when the finger returns to its original position. In Figure 8c, when the CDT is deployed on the wrist, the CDT sensor can react to the twisting and extension of the wrist with a regular electrical signal. At the same time, the CDT sensor reacts regularly and accurately to the motions of the arm and knee (Figure 8d,e).

When the CDT sensor was attached to the neck of the volunteer (Figure 8f), it responds to the strain caused by raising and lowering the head. The CDT sensor could not only monitor large human movements but also accurately respond to the vibration of vocal folds when saying different syllables—“Hola” and “Harbin”, with its excellent pressure-sensitive characteristics. By analyzing the precise sensing signal including the frequency of peaks and the height of peaks in the vocal cord vibration signal, we can interpret the number of words spoken, the frequency of speech, and the volume of speech, which can be utilized to develop technology to help people with a speech impairment to communicate. Therefore, the CDT sensor demonstrates significant potential in the applications such as wearable devices and human–machine interfaces.

3. Conclusion

The high-performance flexible strain sensors were prepared by loading CNTs on electrospun TPU fibrous membranes and demonstrated high sensitivity, wide detection range, good responsiveness, low price, and easy to produce on a large industrial scale. Due to the hydrogen bond interaction and strong interaction between the –OH in the polydopamine layer and the –COOH in the carbon nanotubes, more carbon nanotubes are fixed on the fiber surface and accelerates the migration of CNTs by forming a split-layer structure when the polydopamine layer is stretched, which exhibits a faster change in resistance

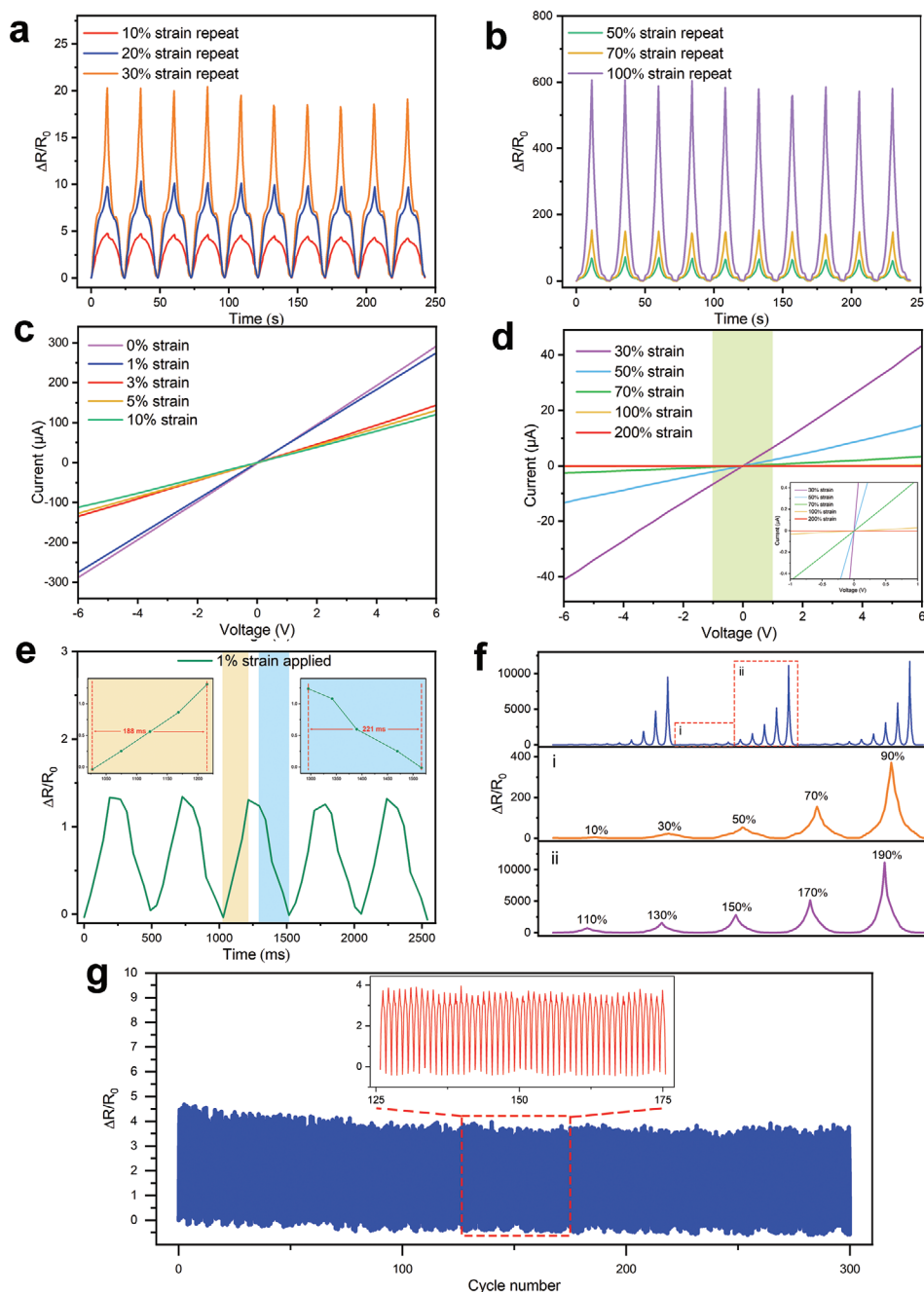


Figure 7. a,b) $\Delta R/R_0$ change of CDT sensor under cyclic stretching at 10–100% strain, c,d) I – V curves of CDT sensor at different micro-strains and large strains, e) CDT sensor response to fast stretching, f) relative resistance change of CDT sensor at different strains for three cycles, g) CDT sensor tested for 300 cycles at 10% strain at a stretching speed of 100 mm min^{-1} .

under stress. A mathematical model constructed by tunnel theory is used to predict the variation of conductive filler and conductive path with strain in CT and CDT samples. We find that the dopamine layer can change the fiber structure of the electrospun membrane and used it to explain the origin of the huge gauge factor of the flexible sensors. Owing to the high sensitivity of CDT sensors, they can be applied to the detection of small strains and various human motions.

4. Experimental Section

Materials: TPU (Elastollan 1185A), density 1.05 g cm^{-3} , was provided by BASF Co., Ltd. Carbon nanotubes (MWCNT-COOH, diameter from 20 to 40 nm, length < 5 microns) were purchased from Shenzhen Nanotech Port Co., Ltd. *N,N*-dimethylformamide (DMF) and tetrahydrofuran (THF) were purchased from Tianjin Fuyu Fine Chemical Co., Ltd. Dopamine hydrochloride (DA·HCl) and Sodium periodate (NaIO_4) were purchased from Shanghai Macklin Biochemical Co., Ltd.

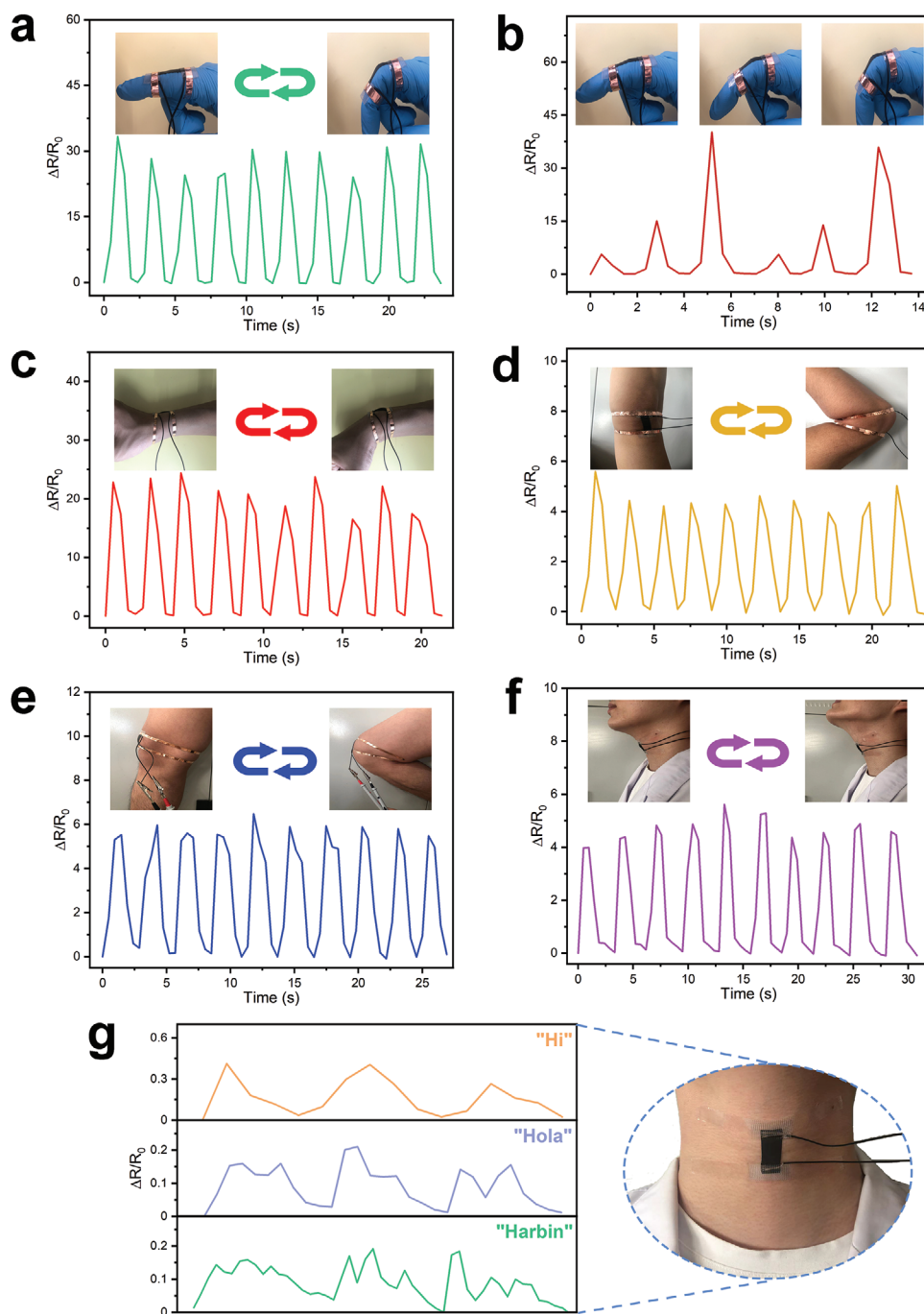


Figure 8. Sensing application of CDT strain sensors in human motion. a) finger flexion, b) finger flexion at 30°, 60°, 90°, c) wrist flexion, d) elbow flexion, e) knee flexion, f) head up and down, g) speaking schematic.

Tris (hydroxymethyl) aminomethane (Tris) was purchased from Fuzhou Feijing Biological Technology Co., Ltd.

Preparation of TPU Fibrous Membrane through Electrospinning: TPU fibrous membranes were prepared using the electrostatic spinning technique. First, TPU particles with a mass fraction of 20% were dissolved in a mixture of DMF/THF (mass ratio of 1:1). The mixture was mechanically stirred at room temperature for 5 h to obtain a homogeneous spinning solution. Then, the spinning solution was injected into a syringe with a capacity of 15 mL for electrostatic spinning. Aluminum foil was chosen to be laid on the roller as the receiving device for TPU fibers, the receiving distance between the needle and receiving

rollers was 20 cm, and electrostatic spinning was carried out at 20 kV and the liquid supply rate was 1 mL h⁻¹. Lastly, the prepared fiber films were dried at 85 °C for 5 h to eliminate the residual organic solvent.

Preparation of Dopamine-Coated TPU Fibrous Membrane: First, the TPU fibrous membrane was repeatedly washed with purified water to eliminate surface pollutants and then dried in an oven at 65 °C for 3 h. The TPU nanofibers mats were coated and finely modified using the fast polydopamine coating method (fPDAC),^[83,84] specifically an aqueous solution of DA/tris (10 mM, pH 8.5) at 2.0 g L⁻¹ and DA with NaIO₄ (10 mM, pH 8.5) with a molar ratio of 0.5 was immediately mixed, and the TPU electrospun membrane was immersed in it

and stirred continuously, and the surface of the TPU electrospun membrane changed from light pink to brown with the spontaneous deposition of the attached polydopamine (PDA) layer. Finally, the PDA-coated TPU fibrous membrane was rinsed with purified water for 30 min and dried in an oven at 65 °C for 3 h to produce the DATPU fibrous membrane.

Preparation of CNTs/TPU and CNTs/DATPU Strain Sensors: First, 2.0 g L⁻¹ of CNTs aqueous solution was sonicated for 2 h to produce a uniformly dispersed CNTs suspension. Then, the TPU electrospun membrane and DATPU film were cut into 50 mm × 50 mm sizes, and the CNTs suspension was filtered onto the TPU electrospun membrane and DATPU film with 2.5, 5, 7.5, 10.5, 15 mL, and a certain amount and rinsed three times with purified water and dried at 80 °C. Finally, filtered CNTs of TPU electrospun membrane and DATPU film were cut into 10 mm × 40 mm segments and connected to wires for the convenience of testing as CT and CDT flexible strain sensors.

Characterization: Scanning electron microscopy (SEM, Volumescape2, Thermo Scientific, America) was employed to observe the morphology of the samples at an accelerating voltage of 5 kV.

Tensile tests were performed with an electronic universal testing apparatus (UTM2203, SUN, China) equipped with a 2 kN transducer at a rate of 50 mm min⁻¹. All specimens are in the size of 40 mm × 10 mm with an applied length of 20 mm. 5 tests were performed on all specimens and the average value was taken.

To acquire the *I*-*V* curves of the sensors, static resistance measurements were performed with a digital source meter (Keithley 2400, USA) at an applied voltage (-6 to + 6 V).

The sensing performance was characterized by the digital source meter (Keithley 2400) in conjunction with a UTM2203 electronic universal testing machine. A sensor sample of size 40 mm × 10 mm was first fixed on the universal mechanical testing machine at a distance of 20 mm from both ends of the fixture, after which the digital source meter was connected to either end of the sensor and used to test the resistance versus strain of the CT and CDT sensors at a constant tensile rate of 10 mm min⁻¹. The relative resistance change can be calculated by Equation (23).

$$\Delta R/R_0 = (R - R_0)/R_0 \quad (23)$$

where *R*₀ is the initial resistance when $\epsilon = 0\%$ and *R* is the real-time resistance that varies with strain.

Informed consent was obtained for all participants involved in the experiments testing the applications of the sensors. In addition, institutional review board approval was not required to perform these experiments.

Acknowledgements

X.Y. and Z.W. contributed equally to this work. This work was supported by Open Project Fund of the Key Laboratory of Engineering Dielectrics and Its Application (2018EDAQY05), Heilongjiang Province Postdoctoral Funded Project (LBH-Q21019), University Nursing Program for Young Scholars with Creative Talents in Heilongjiang Province (UNPYSCT-2018214), Heilongjiang Natural Science Foundation (LH2020E087), and the Engineering and Physical Sciences Research Council (EPSRC, UK) grant-EP/N007921.

Conflict of Interest

The authors declare no conflict of interest.

Data Availability Statement

The data that support the findings of this study are available on request from the corresponding author. The data are not publicly available due to privacy or ethical restrictions.

Keywords

dopamine modification, electrospun, fitted model, flexible sensor

Received: October 29, 2022

Revised: January 18, 2023

Published online:

- [1] N. Wen, L. Zhang, D. Jiang, Z. Wu, B. Li, C. Sun, Z. Guo, *J. Mater. Chem. A* **2020**, *8*, 25499.
- [2] M. Fan, L. Wu, Y. Hu, M. Qu, S. Yang, P. Tang, L. Pan, H. Wang, Y. Bin, *Adv. Compos. Hybrid Mater.* **2021**, *4*, 1039.
- [3] D. Zhang, M. Zhang, J. Wang, H. Sun, H. Liu, L. Mi, C. Liu, C. Shen, *Adv. Compos. Hybrid Mater.* **2022**, *5*, 1812.
- [4] M. Hu, Y. Gao, Y. Jiang, H. Zeng, S. Zeng, M. Zhu, G. Xu, L. Sun, *Adv. Compos. Hybrid Mater.* **2021**, *4*, 514.
- [5] X. Chang, L. Chen, J. Chen, Y. Zhu, Z. Guo, *Adv. Compos. Hybrid Mater.* **2021**, *4*, 435.
- [6] Y. Shen, W. Yang, F. Hu, X. Zhang, Y. Zheng, H. Liu, H. Algadi, K. Chen, *Adv. Compos. Hybrid Mater.* **2023**, *6*, 21.
- [7] X. Liu, Z. Wu, D. Jiang, *Adv. Compos. Hybrid Mater.* **2022**, *5*, 1712.
- [8] J. C. Yang, J. Mun, S. Y. Kwon, S. Park, Z. Bao, S. Park, *Adv. Mater.* **2019**, *31*, 1904765.
- [9] D. J. Lipomi, M. Vosgueritchian, B. C. Tee, S. L. Hellstrom, J. A. Lee, C. H. Fox, Z. Bao, *Nat. Nanotechnol.* **2011**, *6*, 788.
- [10] X. Yue, Y. Jia, X. Wang, K. Zhou, W. Zhai, G. Zheng, K. Dai, L. Mi, C. Liu, C. Shen, *Compos. Sci. Technol.* **2020**, *189*, 108038.
- [11] S. Wang, Y. Fang, H. He, L. Zhang, C. a. Li, J. Ouyang, *Adv. Funct. Mater.* **2020**, *31*, 2007495.
- [12] J. Huang, D. Li, M. Zhao, A. Mensah, P. Lv, X. Tian, F. Huang, H. Ke, Q. Wei, *Adv. Electron. Mater.* **2019**, *5*, 1900241.
- [13] M. Amit, L. Chukoskie, A. J. Skalsky, H. Garudadri, T. N. Ng, *Adv. Funct. Mater.* **2019**, *30*, 1905241.
- [14] T. Q. Trung, N. E. Lee, *Adv. Mater.* **2016**, *28*, 4338.
- [15] Z. Lou, L. Wang, K. Jiang, Z. Wei, G. Shen, *Mater. Sci. Eng., R.* **2020**, *140*, 100523.
- [16] S. Choi, S. I. Han, D. Jung, H. J. Hwang, C. Lim, S. Bae, O. K. Park, C. M. Tschabrunn, M. Lee, S. Y. Bae, J. W. Yu, J. H. Ryu, S. W. Lee, K. Park, P. M. Kang, W. B. Lee, R. Nezafat, T. Hyeon, D. H. Kim, *Nat. Nanotechnol.* **2018**, *13*, 1048.
- [17] H. Lee, T. K. Choi, Y. B. Lee, H. R. Cho, R. Ghaffari, L. Wang, H. J. Choi, T. D. Chung, N. Lu, T. Hyeon, S. H. Choi, D. H. Kim, *Nat. Nanotechnol.* **2016**, *11*, 566.
- [18] H. Joo, Y. Lee, J. Kim, J. S. Yoo, S. Yoo, S. Kim, A. K. Arya, S. Kim, S. H. Choi, N. Lu, H. S. Lee, S. Kim, S. T. Lee, D. H. Kim, *Sci. Adv.* **2021**, *7*, eabd4639.
- [19] K. Xu, Y. Fujita, Y. Lu, S. Honda, M. Shiomi, T. Arie, S. Akita, K. Takei, *Adv. Mater.* **2021**, *33*, 2008701.
- [20] S. C. Mannsfeld, B. C. Tee, R. M. Stoltenberg, C. V. Chen, S. Barman, B. V. Muir, A. N. Sokolov, C. Reese, Z. Bao, *Nat. Mater.* **2010**, *9*, 859.
- [21] D. Wang, Y. Lin, D. Hu, P. Jiang, X. Huang, *Compos. A* **2020**, *130*, 105754.
- [22] Z. Chu, W. Jiao, Y. Huang, Y. Zheng, R. Wang, X. He, *J. Mater. Chem. A* **2021**, *9*, 9634.
- [23] X. Zhou, L. Zhu, L. Fan, H. Deng, Q. Fu, *ACS Appl. Mater. Interfaces* **2018**, *10*, 31655.
- [24] Z. H. Yang, Z. J. Wu, D. W. Jiang, *J. Mater. Chem. C* **2021**, *8*, 11.
- [25] H. Liu, J. Gao, W. Huang, K. Dai, G. Zheng, C. Liu, C. Shen, X. Yan, J. Guo, Z. Guo, *Nanoscale* **2016**, *8*, 12977.
- [26] L. Lin, Y. Choi, T. Chen, H. Kim, K. S. Lee, J. Kang, L. Lyu, J. Gao, Y. Piao, *Chem. Eng. J.* **2021**, *419*, 129513.
- [27] K. Ke, V. Solouki Bonab, D. Yuan, I. Manas-Zloczower, *Carbon* **2018**, *139*, 52.

- [28] M. Amjadi, Y. J. Yoon, I. Park, *Nanotechnology* **2015**, *26*, 375501.
- [29] M. Xu, J. Qi, F. Li, Y. Zhang, *Nanoscale* **2018**, *10*, 5264.
- [30] L. Lu, X. Wei, Y. Zhang, G. Zheng, K. Dai, C. Liu, C. Shen, *J. Mater. Chem. C* **2017**, *5*, 7035.
- [31] F. Guan, Y. Xie, H. Wu, Y. Meng, Y. Shi, M. Gao, Z. Zhang, S. Chen, Y. Chen, H. Wang, Q. Pei, *ACS Nano* **2020**, *14*, 15428.
- [32] G. J. Zhu, P. G. Ren, J. Wang, Q. Duan, F. Ren, W. M. Xia, D. X. Yan, *ACS Appl. Mater. Interfaces* **2020**, *12*, 19988.
- [33] S. Zhang, H. Liu, S. Yang, X. Shi, D. Zhang, C. Shan, L. Mi, C. Liu, C. Shen, Z. Guo, *ACS Appl. Mater. Interfaces* **2019**, *11*, 10922.
- [34] R. Yin, S. Yang, Q. Li, S. Zhang, H. Liu, J. Han, C. Liu, C. Shen, *Sci. Bull.* **2020**, *65*, 899.
- [35] D. Jiang, Y. Wang, B. Li, C. Sun, Z. Wu, H. Yan, L. Xing, S. Qi, Y. Li, H. Liu, W. Xie, X. Wang, T. Ding, Z. Guo, *Polym. Rev.* **2019**, *304*, 1900074.
- [36] Y. Zhou, P. Zhan, M. Ren, G. Zheng, K. Dai, L. Mi, C. Liu, C. Shen, *ACS Appl. Mater. Interfaces* **2019**, *11*, 7405.
- [37] Z. Niu, W. Yuan, *ACS Appl. Mater. Interfaces* **2021**, *13*, 4508.
- [38] M. Qu, H. Wang, Q. Chen, L. Wu, P. Tang, M. Fan, Y. Guo, H. Fan, Y. Bin, *Chem. Eng. J.* **2022**, *427*, 131648.
- [39] J. S. Heo, R. Soleymanpour, J. Lam, D. Goldberg, E. Large, S. K. Park, I. Kim, *IEEE J. Biomed. Health Inf.* **2022**, *26*, 581.
- [40] Y. Fei, F. Chen, W. Fang, A. Hejna, L. Xu, T. Liu, M. Zhong, J. Yang, T. Kuang, *J. Mater. Chem. C* **2021**, *9*, 13103.
- [41] B. Li, J. Luo, X. Huang, L. Lin, L. Wang, M. Hu, L. Tang, H. Xue, J. Gao, Y.-W. Mai, *Compos. B* **2020**, *181*, 107580.
- [42] Q. Zheng, J.-h. Lee, X. Shen, X. Chen, J.-K. Kim, *Mater. Today* **2020**, *36*, 158.
- [43] Y. Li, T. He, L. Shi, R. Wang, J. Sun, *ACS Appl. Mater. Interfaces* **2020**, *12*, 17691.
- [44] L. Q. Tao, K. N. Zhang, H. Tian, Y. Liu, D. Y. Wang, Y. Q. Chen, Y. Yang, T. L. Ren, *ACS Nano* **2017**, *11*, 8790.
- [45] M. Qu, F. Nilsson, Y. Qin, G. Yang, Y. Pan, X. Liu, G. Hernandez Rodriguez, J. Chen, C. Zhang, D. W. Schubert, *Compos. Sci. Technol.* **2017**, *150*, 24.
- [46] L. V. Kayser, D. J. Lipomi, *Adv. Mater.* **2019**, *31*, 1806133.
- [47] X. Wang, J. Zhou, Y. Zhu, W. Cheng, D. Zhao, G. Xu, H. Yu, *Chem. Eng. J.* **2020**, *392*, 123644.
- [48] E. Roh, B. U. Hwang, D. Kim, B. Y. Kim, N. E. Lee, *ACS Nano* **2015**, *9*, 6252.
- [49] G. Ge, Y. Cai, Q. Dong, Y. Zhang, J. Shao, W. Huang, X. Dong, *Nanoscale* **2018**, *10*, 10033.
- [50] Y. Zheng, R. Yin, Y. Zhao, H. Liu, D. Zhang, X. Shi, B. Zhang, C. Liu, C. Shen, *Chem. Eng. J.* **2021**, *420*, 127720.
- [51] W. Chen, L. X. Liu, H. B. Zhang, Z. Z. Yu, *ACS Nano* **2021**, *15*, 7668.
- [52] X. Zheng, J. Shen, Q. Hu, W. Nie, Z. Wang, L. Zou, C. Li, *Nanoscale* **2021**, *13*, 1832.
- [53] N. Bhardwaj, S. C. Kundu, *Biotechnol. Adv.* **2010**, *28*, 325.
- [54] H. Yoshimoto, Y. M. Shin, H. Terai, J. P. Vacanti, *Biomater* **2003**, *24*, 2077.
- [55] Y. Qin, D. W. Schubert, *Polymer* **2019**, *181*, 121769.
- [56] H. Ziyadi, M. Baghali, M. Bagherianfar, F. Mehrali, R. Faridi-Majidi, *Adv. Compos. Hybrid Mater.* **2021**, *4*, 768.
- [57] Z. Zhang, Y. Zhao, Z. Li, L. Zhang, Z. Liu, Z. Long, Y. Li, Y. Liu, R. Fan, K. Sun, Z. Zhang, *Adv. Compos. Hybrid Mater.* **2022**, *5*, 513.
- [58] M. Ren, Y. Zhou, Y. Wang, G. Zheng, K. Dai, C. Liu, C. Shen, *Chem. Eng. J.* **2019**, *360*, 762.
- [59] Y. X. Song, W. M. Xu, M. Z. Rong, M. Q. Zhang, *Adv. Compos. Hybrid Mater.* **2022**, *5*, 513.
- [60] R. Liu, J. G. Kim, P. Dhakal, W. Li, J. Ma, A. Hou, C. Merkel, J. Qiu, M. Zoran, S. Wang, *Adv. Compos. Hybrid Mater.* **2023**, *6*, 14.
- [61] S. Sharafkhani, M. Kokabi, *Adv. Compos. Hybrid Mater.* **2022**, *5*, 3081.
- [62] M. Liu, H. Wu, Y. Wu, P. Xie, R. A. Pashameah, H. M. Abo-Dief, S. M. El-Bahy, Y. Wei, G. Li, W. Li, G. Liang, C. Liu, K. Sun, R. Fan, *Adv. Compos. Hybrid Mater.* **2022**, *5*, 2021.
- [63] P. Wang, T. S. , H. M. A.-D. , J. Song, A. K. Alanazi, B. Fan, M. Huang, Z. Lin, A. A. Altalhi, S. Gao, L. Yang, J. Liu, S. Feng, T. Cao, *Adv. Compos. Hybrid Mater.* **2022**, *5*, 1100.
- [64] Z. Yan, S. Wang, J. Bi, Q. He, H. Song, I. H. E. Azab, S. M. El-Bahy, A. Y. Elnaggar, M. Huang, M. H. H. Mahmoud, J. Wang, Q. Shao, *Adv. Compos. Hybrid Mater.* **2019**, *5*, 2116.
- [65] L. Song, J. Chen, B. B. Xu, Y. Huang, *ACS Nano* **2021**, *15*, 12.
- [66] B. B. Xu, Q. Liu, Z. Suo, R. C. Hayward, *Adv. Funct. Mater.* **2016**, *26*, 3218.
- [67] H. Wei, Z. Wang, H. Zhang, Y. Huang, Z. Wang, Y. Zhou, B. B. Xu, S. Halila, J. Chen, *Chem. Mater.* **2021**, *33*, 17.
- [68] X. Dai, Y. Du, Y. Wang, Y. Liu, N. Xu, Y. Li, D. Shan, B. B. Xu, J. Kong, *ACS Appl. Polym. Mater.* **2020**, *2*, 3.
- [69] Z. Wang, H. Zhou, D. Liu, X. Chen, D. Wang, S. Dai, F. Chen, B. B. Xu, *Adv. Funct. Mater.* **2022**, *32*, 2201396.
- [70] Y. Liu, A. Sun, S. Sridhar, Z. Li, Z. Qin, J. Liu, X. Chen, H. Lu, B. Z. Tang, B. B. Xu, *ACS Appl. Mater. Interfaces* **2021**, *13*, 30.
- [71] Z. Li, Y. Liu, M. Lei, A. Sun, S. Sridhar, Y. Li, X. Liu, H. Lu, Y. Q. Fu, B. B. Xu, *Soft Matter* **2020**, *16*, 1636.
- [72] H. Li, J. Chen, X. Chang, Y. Xu, G. Zhao, Y. Zhu, Y. Li, *J. Mater. Chem. A* **2021**, *9*, 1795.
- [73] C. Lozano-Pérez, J. V. Cauich-Rodríguez, F. Avilés, *Compos. Sci. Technol.* **2016**, *128*, 25.
- [74] Y. Wang, Y. Jia, Y. Zhou, Y. Wang, G. Zheng, K. Dai, C. Liu, C. Shen, *J. Mater. Chem. C* **2018**, *6*, 8160.
- [75] X. Wang, X. Liu, D. W. Schubert, *Nanomicro Lett.* **2021**, *13*, 64.
- [76] J. Lin, W. Wang, J. Cheng, Z. Cui, J. Si, Q. Wang, W. Chen, *J. Appl. Polym. Sci.* **2020**, *137*, 49252.
- [77] Y. Li, B. Zhou, G. Zheng, X. Liu, T. Li, C. Yan, C. Cheng, K. Dai, C. Liu, C. Shen, Z. Guo, *J. Mater. Chem. C* **2018**, *6*, 2258.
- [78] J. F. Guan, J. Zou, P. Y. Liu, Y. X. Jiang, G. J. Yu, *Ecotoxicol. Environ. Saf.* **2020**, *201*, 110872.
- [79] H. Bi, Y. Li, S. Liu, P. Guo, Z. Wei, C. Lv, *Sens. Actuators* **2018**, *171*, 1132.
- [80] G. Xu, B. Li, T. X. Cui, L. Ling, X. Luo, *Sens. Actuators, B* **2018**, *188*, 405.
- [81] X.-W. Zhang, Y. Pan, Q. Zheng, X.-S. Yi, *J. Polym. Sci. B* **2000**, *38*, 2739.
- [82] S. Zhao, D. Lou, G. Li, Y. Zheng, G. Zheng, K. Dai, C. Liu, Y. Jiang, C. Shen, *Compos. Sci. Technol.* **2018**, *163*, 18.
- [83] S. H. Hong, S. Hong, M.-H. Ryou, J. W. Choi, S. M. Kang, H. Lee, *Adv. Mater. Interfaces* **2016**, *3*, 1500857.
- [84] J. Wang, H. Guo, X. Shi, Z. Yao, W. Qing, F. Liu, C. Y. Tang, *J. Colloid Interface Sci.* **2019**, *535*, 239.